




ARTICLE

DOI: 10.1038/s42005-018-0056-x

OPEN

Nanoscale spin-wave circuits based on engineered reconfigurable spin-textures

Edoardo Albisetti ^{1,2}, Daniela Petti ², Giacomo Sala², Raffaele Silvani^{3,4}, Silvia Tacchi³, Simone Finizio⁵, Sebastian Wintz⁵, Annalisa Calò¹, Xiaorui Zheng¹, Jörg Raabe ⁵, Elisa Riedo^{1,6} & Riccardo Bertacco^{2,7}

Magnonics is gaining momentum as an emerging technology for information processing. The wave character and Joule heating-free propagation of spin-waves hold promises for highly efficient computing platforms, based on integrated magnonic circuits. The realization of such nanoscale circuitry is crucial, although extremely challenging due to the difficulty of tailoring the nanoscopic magnetic properties with conventional approaches. Here we experimentally realize a nanoscale reconfigurable spin-wave circuitry by using patterned spin-textures. By space and time-resolved scanning transmission X-ray microscopy imaging, we directly visualize the channeling and steering of propagating spin-waves in arbitrarily shaped nanomagnonic waveguides, with no need for external magnetic fields or currents. Furthermore, we demonstrate a prototypic circuit based on two converging nanowaveguides, allowing for the tunable spatial superposition and interference of confined spin-waves modes. This work paves the way to the use of engineered spin-textures as building blocks of spin-wave based computing devices.

¹Advanced Science Research Center, CUNY Graduate Center, 85 St. Nicholas Terrace, New York, NY 10031, USA. ²Dipartimento di Fisica, Politecnico di Milano, via G. Colombo 81, 20133 Milano, Italy. ³Istituto Officina dei Materiali del CNR (CNR-IOM), Unità di Perugia, c/o Dipartimento di Fisica e Geologia, via A. Pascoli, 06123 Perugia, Italy. ⁴Dipartimento di Fisica e Geologia, Università di Perugia, Via A. Pascoli, 06123 Perugia, Italy. ⁵Paul Scherrer Institute, Forschungsstrasse 111, 5232 Villigen, PSI, Switzerland. ⁶Tandon School of Engineering, New York University (NYU), 6 MetroTech Center, Brooklyn, NY 11201, USA. ⁷IFN-CNR, c/o Politecnico di Milano, Piazza Leonardo da Vinci, 32, 20133 Milano, Italy. Correspondence and requests for materials should be addressed to E.A. (email: edoardo.albisetti@polimi.it) or to D.P. (email: daniela.petti@polimi.it)

The manipulation of spin-waves represents a promising alternative to conventional electronics for the development of energy-efficient computing platforms. In the last few years, many concepts of spin-wave based devices have been proposed^{1–19}. However, the experimental realization of a nanoscale spin-wave circuitry for guiding, manipulating, and controlling the interference of magnons, which is the basis for realizing nanomagnonic devices, is still missing. A major challenge is the efficient channeling and steering of spin-waves, which so far has been achieved in micron sized elements using external fields^{20–24} or arrays of nanomagnets²⁵. In the route toward nanomagnonics, the use of nanoscale spin-textures for controlling the propagation of spin-waves is highly appealing. Recently, the concept of spin-wave channeling within domain walls has been theoretically proposed^{26–28}, and experimental evidence for spin-wave confinement at a domain wall has been provided on a straight wall stabilized via shape anisotropy²⁹. However, so far, the difficulty of engineering the spin-texture at the nanoscale with conventional techniques has hindered the realization and investigation of magnonic circuits based on domain walls. In particular, the steering of spin-waves by means of curved domain walls and the use of complex spin-textures for controlling the interference of multiple modes propagating within a nanoscale spin-wave circuitry remain elusive. Furthermore, the direct observation and a detailed investigation of these confined spin-wave modes are still missing.

In this work, we demonstrate the fundamental building blocks of spin-waves circuitry, i.e., arbitrarily shaped magnonic nanowaveguides and a prototypic spin-wave circuit allowing for the tunable superposition of signals propagating in two converging waveguides, by patterning the spin-texture of a ferromagnetic thin film via thermally assisted magnetic scanning probe lithography (tam-SPL)^{30,31}. The absence of a physical patterning and the reversibility of tam-SPL allows the realization of fully reconfigurable nanomagnonic structures based on spin-textures with engineered functionality. Through space and time-resolved scanning transmission X-ray microscopy (STXM), we provide direct evidence for the channeling and steering of localized spin-wave modes propagating along straight and curved domain wall-based waveguides, with no need for an applied bias magnetic field. Furthermore, we demonstrate the tunable spatial superposition and interference of confined spin-wave modes propagating within two converging nanoscale waveguides. The experimental realization of reconfigurable nanomagnonic circuits based on domain walls paves the way to the use of engineered spin-textures as building blocks of spin-wave based computing devices.

Results

Experimental protocol and sample structure. In Fig. 1, we report a sketch of the experiments. Different spin-textures were patterned in an exchange bias ferromagnet/antiferromagnet bilayer (Fig. 1a), by sweeping a heated scanning probe in an external magnetic field for setting the unidirectional magnetic anisotropy strength and direction in the ferromagnetic film. This allows for the nanopatterning of engineered spin-configurations, as in the case of the curved 180° Néel domain wall of Fig. 1a, which is stabilized by patterning two magnetic domains with antiparallel remanent magnetization. Straight and curved domain walls, as well as complex spin-textures comprising two converging domain walls, were obtained by controlling the geometry of the area scanned by the tip. Spin-waves were excited by injecting a radio frequency (RF) current in a microstrip antenna. Static and time-resolved images with magnetic contrast were acquired via STXM by measuring the transmitted X-ray intensity, so that the

X-ray magnetic circular dichroism (XMCD) provides contrast to the in-plane component of the magnetization M_x (Fig. 1b) (Methods section).

The configuration of the spin-wave modes is shown in Fig. 1c. Spin-waves are confined in the transverse direction of the wall by the reduced local effective field arising from the inhomogeneous magnetization profile, and propagate freely along the wall^{26,29}. Such modes, called Winter magnons^{26,32,33}, are characterized by an elliptical precession of the spins along the wall, with the major axis lying in the film plane, associated to a propagating flexural motion of the wall profile, analogous to transverse elastic waves on a string.

Figure 2a, b shows the sample structure, consisting of an exchange bias $\text{Co}_{40}\text{Fe}_{40}\text{B}_{20}$ 20 nm/ $\text{Ir}_{22}\text{Mn}_{78}$ 10 nm/ Ru 2 nm multilayer³⁴, and the optical image of the sample. The white dashed line indicates the orientation of a patterned domain wall with respect to the antenna.

In Fig. 2c–e, the static STXM images of the spin-textures patterned via tam-SPL are reported, where the dark (bright) contrast corresponds to $M_x > 0$ (< 0). The black region at the bottom of the figure shows the boundary of the microstrip. For the straight and parabolic domain walls of Fig. 2c, d, respectively, the images acquired at zero external field display sharp 180° Néel walls. The corresponding micromagnetic simulations (Fig. 2f, g) show a 180° spin rotation within the sample plane, with the central spins (white regions) defining the domain wall profile lying along the y -axis^{30,35}.

Figure 2e shows the static image of a more complex spin-texture comprising two 180° Néel walls tilted by a 30° angle from each other, sharing a common apex. In this case, a static 1.5 mT magnetic field was applied in the x -direction in order to precisely control the distance between the two domain walls and the position of the apex (see discussion below). The image of the same structure acquired at remanence is shown in Supplementary Figure 1. The corresponding micromagnetic simulation (Fig. 2h) shows that the two domains walls merge at the intersection, where the magnetization orientation is determined by the spin configuration of the two walls. After the intersection, a narrow “transition” region is formed, where the magnetization rotates continuously until a uniform magnetization orientation is reached within the domain.

Spin-wave propagation along patterned domain walls. Spin-waves were imaged stroboscopically via time-resolved STXM (Methods). In Fig. 3, the results for straight and curved domain walls are reported. Figure 3a shows snapshots of the normalized M_x contrast for the straight wall, calculated as the magnetic deviation $\Delta M_x(t)$ from the time-averaged state $M_x(t)$, acquired at different times within a single period^{7,36}. A Gaussian filtering was used for enhancing the contrast (see Supplementary Note 2, Supplementary Table 1 and Supplementary Movie 1, 2 for video and raw data video). The excitation frequency was 1.28 GHz and no static external magnetic field was applied. The normalized M_x contrast shows spin-waves confined at the domain wall and propagating away from the antenna located at the bottom of the panels.

The spatial map of the amplitude of the spin-wave excitation is reported in Fig. 3b. The map is obtained by fitting the time-trace of each acquired pixel (raw data) with a sinusoidal function, and plotting for each pixel the amplitude of the corresponding fit (see Supplementary Note 3 and Supplementary Figure 2). Both Fig. 3b and the horizontal profile extracted from it at $x = 1.1 \mu\text{m}$ from the stripline (Fig. 3c) show that the mode is confined at the domain wall, with a lateral extension (FWHM) of 120 nm. In order to demonstrate the propagating character of the spin-waves,

the time-traces (sinusoidal fitting) related to pixels located within the domain wall at different distances from the antenna are plotted as a function of time (Fig. 3d). The time delay observed

when moving away from the antenna corresponds to a linear phase shift with distance (Fig. 3e), clearly confirming the

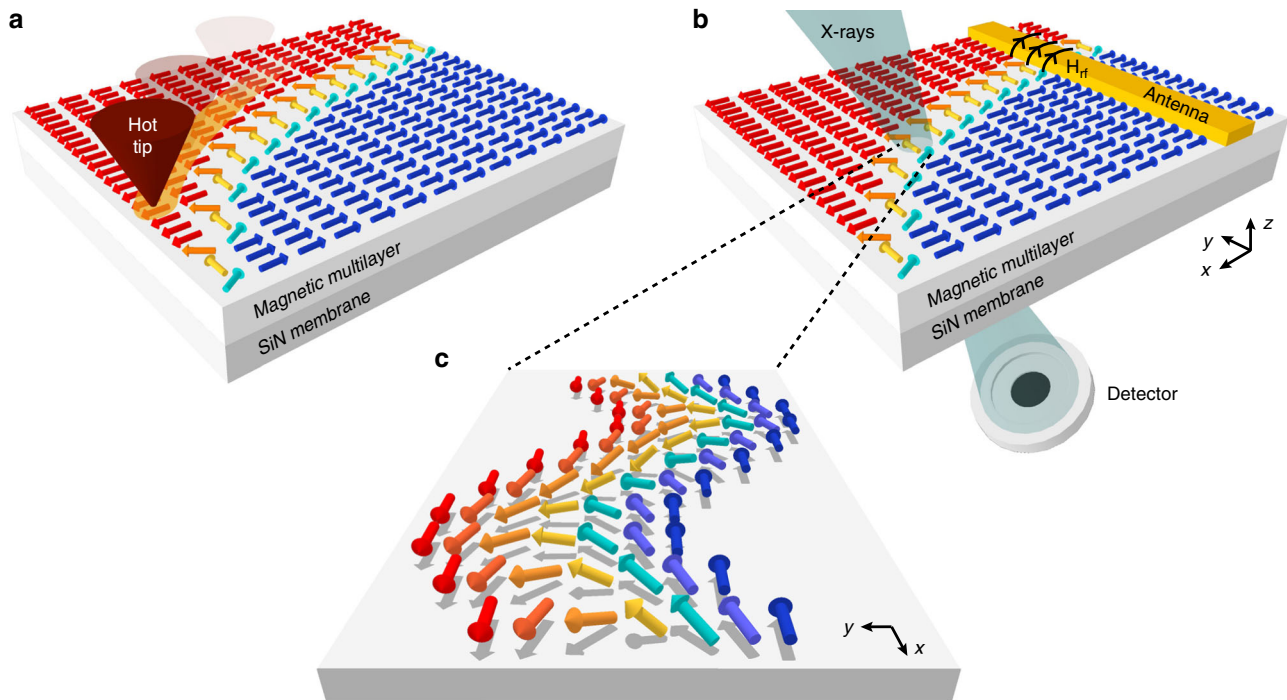


Fig. 1 Patterning of nanoscale spin-textures and study of the confined spin-wave modes. **a** Nanoscale spin-textures, such as magnetic domain walls with tailored spin configuration, are patterned via thermally assisted magnetic scanning probe lithography (tam-SPL) in a continuous exchange biased ferromagnetic layer. **b** The static characterization of the patterned spin-textures and the study of the localized spin-wave modes are performed via scanning transmission X-ray microscopy (STXM). A microstrip antenna is employed for the spin-wave excitation. **c** Schematic representation of a spin-wave mode confined at a 180° Néel domain wall, propagating freely along the wall

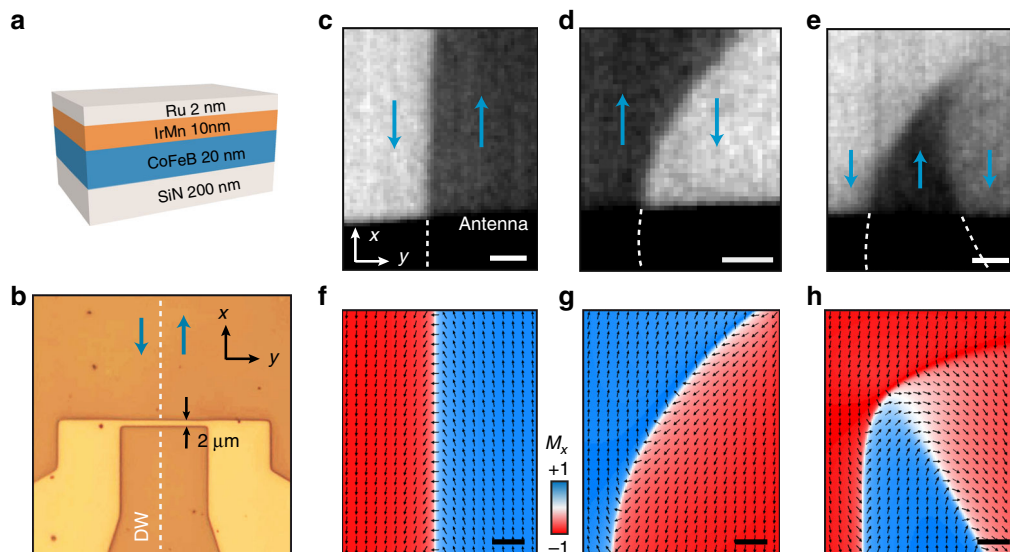


Fig. 2 Sample structure, static characterization, and micromagnetic simulations of the patterned spin-textures. **a** Structure of the studied samples, consisting of a CoFeB 20 nm/IrMn 10 nm continuous exchange bias bilayer. **b** Optical image of the sample, showing a $2\ \mu\text{m}$ wide microstrip antenna for spin-wave excitation. The white dashed line indicates the position of a straight patterned domain wall, with respect to the antenna. Blue arrows indicate the direction of the CoFeB magnetization within the domains. **c–e** Static scanning transmission X-ray microscopy (STXM) images of a straight 180° Néel domain wall, a parabola-shaped 180° Néel wall, and a complex spin-texture comprising two converging 180° Néel walls sharing a common apex, respectively. The black (white) contrast indicates $M_x > 0$ (< 0), confirming the stabilization of sharp Néel walls. The arrows indicate the direction of the magnetization within the domains. The dashed lines indicate the continuation of the domain walls under the antenna. No external magnetic field was applied for **c** and **d**. In **e**, a 1.5 mT field was applied along $+x$ for controlling the distance between the two domain walls and the position of the apex. **f–h** Micromagnetic simulations corresponding to the upper panels. The black arrows indicate the local spin configuration. The blue (red) color indicates $M_x > 0$ (< 0). Scale bars: 500 nm

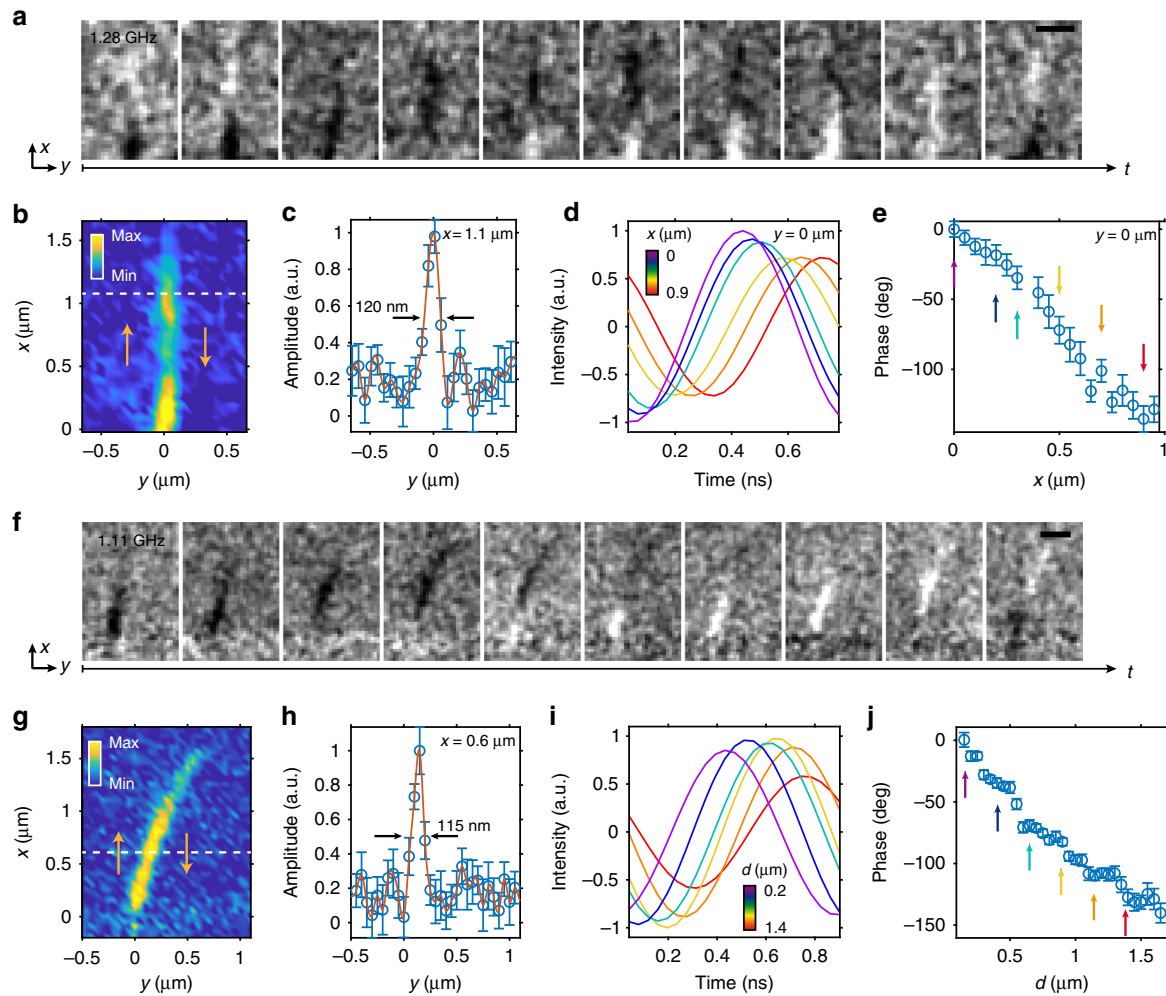


Fig. 3 Localized spin-waves propagating along straight and curved domain walls. **a, f** Normalized time-resolved scanning transmission X-ray microscopy (STXM) images showing the propagation of localized spin-waves along a straight 180° Néel wall and a parabola-shaped 180° Néel wall, respectively. The frequency of the excitation current was 1.28 GHz (1.11 GHz) for the straight (curved) wall. **b, g** Spatial maps of the spin-wave excitation amplitude, showing localization at the domain wall for the straight and curved walls. The arrows indicate the direction of the magnetization within the domains. The $x = 0$, $y = 0$ position is set in correspondence of the wall, right outside the antenna. **c, h** Horizontal profiles extracted from **b** and **g** in correspondence of the white dashed lines. The full width at half maximum (FWHM) of the excitation peaks in correspondence of the domain wall is 120 nm **c** and 115 nm **h**. The error bars are calculated from the sinusoidal fitting. **d, i** STXM time traces (sinusoidal fitting) showing the excitation at different distances from the antenna, color-coded, along the domain wall for the straight and curved walls. **e, j** Phase analysis as a function of distance from the antenna along the straight and curved domain wall confirming the propagating character of the spin-waves, respectively. Color-coded arrows indicate the corresponding time traces of **d** and **i**, respectively. Scale bars: 500 nm

propagating character of the mode and allowing to estimate its wave vector.

Spin-waves propagating along a curved path, at remanence, are shown in the snapshots of Fig. 3f, extracted from Supplementary Movie 3 (see Supplementary Movie 4 for the raw data and Supplementary Table 3, Supplementary Movie 13, 14 for the $M_x(t)$). The excitation frequency was 1.11 GHz. A Gaussian filtering was used for enhancing the contrast. The mode is confined at the wall and follows its profile, showing a lateral extension of 115 nm (Fig. 3g, h). Both the sinusoidal fits (of raw data) as a function of time (Fig. 3i) and the phase analysis of Fig. 3j confirm the propagating nature of the mode. Figure 3 shows spin-waves confined at the patterned walls detected up to $2\ \mu\text{m}$ away from the antenna. Longer propagation distances are reported in Supplementary Movies 5, 6, where we show spin-waves propagating along a curved domain wall and clearly detectable up to $3.5\ \mu\text{m}$ from the microstrip.

Micromagnetic simulations of the confined spin-wave modes are presented in Fig. 4 (see Methods and Supplementary Figure 3 for details). Figure 4a, b shows micromagnetic simulations for the straight (curved) wall, carried out at remanence, driven by a line source of sinusoidal magnetic field at 1.28 GHz (1.11 GHz), as in the experimental data of Fig. 3. The M_x and M_z components are reported in the left and right panels, respectively, while the magnetic deviation $\Delta M_x(t)$ from the time averaged value $\langle M_x(t) \rangle$, which corresponds to the STXM signal reported in Fig. 3, is shown in the central panel. The flexural motion of the wall, associated with the spin precession within the wall, can be observed for both straight and curved geometries. In good agreement with the experimental results, these findings indicate that wall-bound Winter-like modes, propagating along the wall, can be excited in both the straight and curved geometries.

Figure 4c reports the dispersion relation simulated for spin-waves confined at a straight 180° Néel domain wall, together with the experimental one. The simulations were performed with the

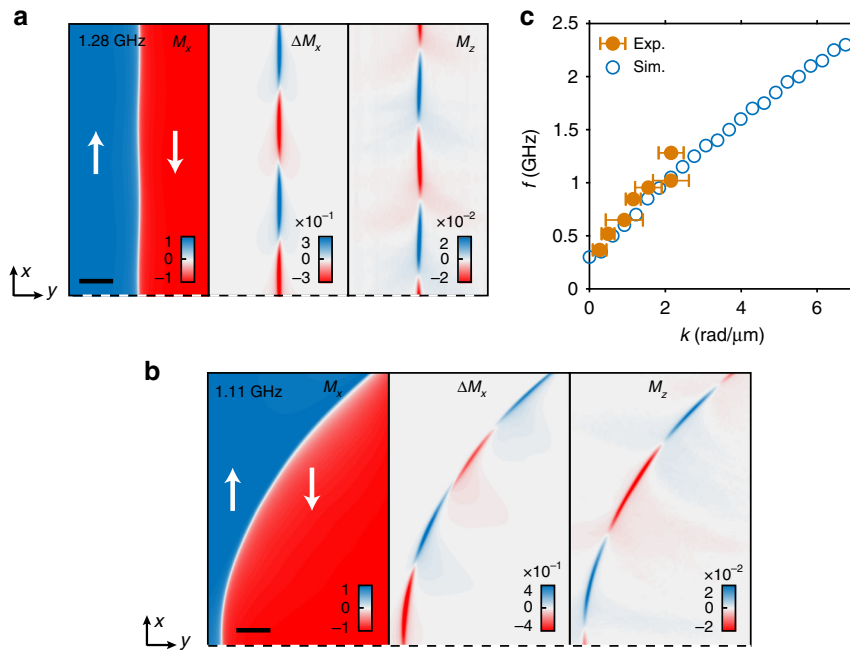


Fig. 4 Spin-wave modes, simulated and experimental dispersion. **a, b** Micromagnetic simulations of the spin-waves mode in presence of a straight Néel 180° domain wall and in presence of a curved Néel 180° wall, respectively. The excitation (frequency indicated in each panel) is generated by a horizontal line antenna placed below the dashed line. From the left to the right, the M_x , the ΔM_x and the M_z are shown. The mode is characterized by the flexural motion of the domain wall in the plane of the film and by the precession of the spins along the domain wall. The arrows indicate the direction of the magnetization within the domains. Scale bars: 500 nm. **c** Dispersion of the spin-waves confined at the straight domain wall. Empty blue (filled orange) circles represent the simulated (experimental) dispersion

same geometry as in Fig. 4a, but using a sinc-shaped field pulse as excitation (Methods). The experimental values of the wave vector were extracted from the linear fitting of the phase shift vs. distance curves obtained from experiments performed at different excitation frequencies (see discussion for Fig. 3 and Supplementary Note 3).

In good agreement with the experimental results, the simulations confirm the propagating character of the excitations, showing a positive dispersion and the presence of a small bandgap below 0.3 GHz, which can be ascribed to the residual effective field within the domain wall due to exchange bias and uniaxial anisotropies²⁶. The simulated (experimental) spin-wave group velocity $v_g = \partial\omega/\partial k$, extracted at $k \rightarrow 0$, is $v_{gSim} = 2.30 \pm 0.34 \text{ km s}^{-1}$ ($v_{gExp} = 2.77 \pm 1.4 \text{ km s}^{-1}$). Noteworthy, the demonstration of the propagating character and of the positive dispersion confirms that such guided modes can be used for transporting information within integrated nanomagnonic circuits.

Waveguides for efficiently controlling and manipulating confined spin-wave modes constitute fundamental building blocks for the realization of nanomagnonic devices. In the following, we demonstrate a nanomagnonic circuit allowing for the tunable spatial superposition and interference of guided spin-wave modes propagating in two converging waveguides.

Tunable spatial superposition of confined modes. Figure 5a shows the STXM images of a spin-texture comprising two domain walls (see also Fig. 2e). By applying a small static magnetic field in the $-x$ -direction, ranging from 2 mT to 1.68 mT, the distance between the two domain walls (dashed white lines) can be controlled. In the top panel, the two domain walls are spatially separate. By decreasing the field, the two walls are brought closer

(central panel) and finally converge at the common apex (lower panel).

Figure 5b shows STXM snapshots from the three different configurations for a 1.28 GHz excitation frequency. The images were smoothed with a gaussian filter for increasing contrast (see Supplementary Note 2, Supplementary Table 2 and Supplementary Movie 7–12 for the videos and raw data). The normalized M_x contrast shows, in all three cases, two guided spin-wave modes propagating from the antenna with different relative phases. These two modes, which are spatially separate close to the antenna, approach as the domain walls converge, and partially overlap for low applied fields. In order to better visualize the progressive overlapping of the two modes, each pixel of the data of Fig. 5b was fitted with a sinusoidal function (see Supplementary Note 3 and the discussion of Fig. 3). Figure 5c shows the amplitude of the sinusoidal fit along the horizontal profiles of Fig. 5a (green dashed lines), in the three configurations. The two peaks, with full width at half maximum (FWHM) of around 200 nm, correspond to the two guided modes. For an applied magnetic field of 2 mT, the two modes are separated by 810 nm and do not overlap. By decreasing the field down to 1.68 mT, the two modes are brought closer and to partially overlap, with a peak-to-peak distance of 340 nm.

In the top panels of Fig. 5d the sinusoidal fits along the horizontal profiles of Fig. 5a (green dashed lines) are plotted as a function of time for the different applied fields. In the bottom panels, single sinusoidal profiles are extracted from the positions marked by the color-coded stars in the top panels. Blue and yellow curves show the magnetization dynamics in correspondence of the maximum amplitude of the two guided modes. As expected, their phase difference depends on the applied field, because of the modulation of the waveguide geometry and spin configuration.

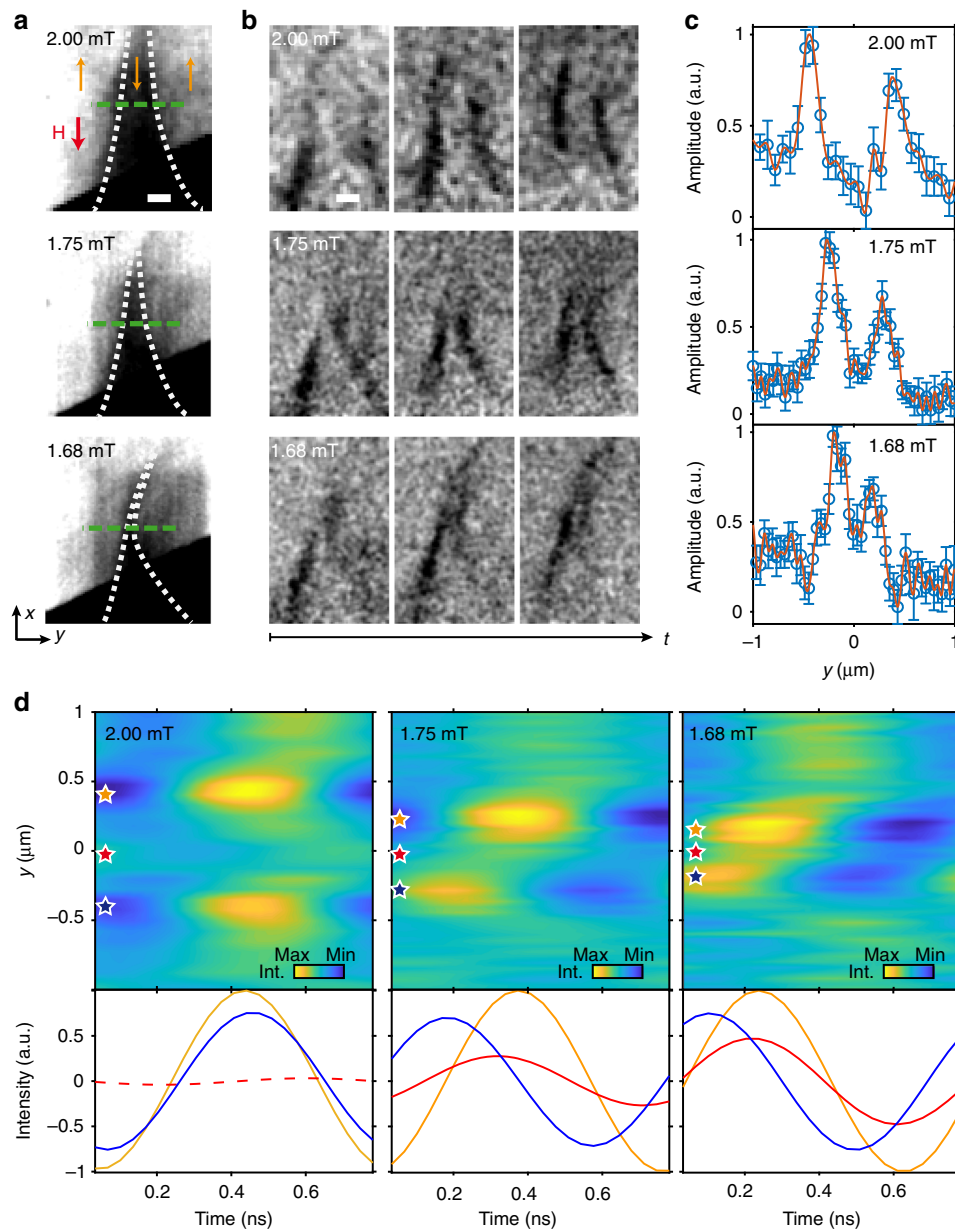


Fig. 5 Tunable spatial superposition of two modes via external fields. **a** Scanning transmission X-ray microscopy (STXM) images of a spin-texture consisting of two 180° Néel domain walls sharing a common apex, for different external magnetic fields applied in the $-x$ -direction (red arrow). The distance between the two domain walls, marked by dashed white lines, is controlled by the external field. Orange arrows indicate the direction of the magnetization within the domains. **b** Normalized time-resolved STXM images showing spin-waves excited at 1.28 GHz propagating along the two domain walls, for different external fields, indicated at the top of each panel. **c** Spin-wave excitation amplitude as a function of the distance along the horizontal profiles indicated by the green dashed lines in **a**, for different external fields. The error bars are calculated from the sinusoidal fitting. **d** In the top panels, STXM time traces (sinusoidal fitting) as a function of y , along the horizontal profiles marked by the green dashed lines in **a**, for different external fields. In the bottom panels, time-traces extracted in correspondence of the color-coded stars in the panel above. For 2 mT the modes are spatially separate. By reducing the external field, a tunable spatial superposition of the two modes is achieved as shown by the increasing excitation amplitude at $y = 0 \mu\text{m}$ for 1.75 mT and 1.68 mT. Scale bars: 500 nm

The red curves show the dynamics in the region where the two modes overlap. For 2.00 mT (left panel), the two modes are spatially separate, therefore at $y = 0$ no excitation is measured (red dashed line). For lower fields (central and right panels), we observe a sizeable modulation of the excitation amplitude and phase in the overlap region, which arises from the tuning of the spatial superposition of the two guided modes. We anticipate that the control of the superposition, phase difference and amplitude of the guided modes via external stimuli such as fields or current, allows to envision the implementation of logic functions in spin-

texture based devices, such as Mach-Zehnder-type spin-wave interferometers⁹.

Discussion

In this work, we experimentally realized the fundamental building blocks of a reconfigurable spin-wave circuitry based on patterned spin-textures, i.e. arbitrarily shaped magnonic nanowaveguides. We directly imaged and studied via space and time-resolved STXM the channeling and steering of spin-waves propagating within nanoscale straight and curved paths, without the need for

external applied fields. Furthermore, we realized a prototypical nanomagnonic circuit allowing for the tunable spatial superposition of signals propagating in two converging waveguides. The experimental realization of a reconfigurable nanoscale circuitry allowing for the steering, manipulation and controlled interference of spin-waves has been a long-standing challenge. This work clearly demonstrates that engineered spin-textures represent a powerful, versatile tool for realizing such a circuitry, marking a fundamental step toward the development of integrated nanomagnonic computing devices.

Methods

Sample fabrication. $\text{Co}_{40}\text{Fe}_{40}\text{B}_{20}$ 20 nm/ $\text{Ir}_{22}\text{Mn}_{78}$ 10 nm/ Ru 2 nm stacks were deposited on 200 nm thick Si_3N_4 membranes by DC magnetron sputtering using an AJA Orion8 system with a base pressure below 1×10^{-8} Torr. During the deposition, a 30 mT magnetic field was applied in the sample plane for setting the magnetocrystalline uniaxial anisotropy direction in the CoFeB layer and the exchange bias direction in the as-grown sample. Then, the samples underwent an annealing in vacuum at 250 °C for 5 min, in a 400 mT magnetic field oriented in the same direction as the field applied during the growth. The resulting exchange bias field was 2.5 mT.

Thermally assisted magnetic Scanning Probe Lithography (tam-SPL) was performed via NanoFrazor Explore (SwissLitho AG). Spin-textures were patterned by sweeping in a raster-scan fashion the scanning probe, heated above the blocking temperature of the exchange bias system $T_B \approx 300$ °C, in presence of an external magnetic field. Two rotatable permanent magnets were employed for generating a uniform external magnetic field applied in the sample plane during patterning.

$2 \mu\text{m} \times 30 \mu\text{m}$ microstrip antennas were then fabricated via optical lithography using a Heidelberg MLA100 Maskless Aligner and lift-off, after depositing a 50 nm thick SiO_2 insulating layer via magnetron sputtering. A Cr 5 nm/ Cu 200 nm bilayer was deposited by means of thermal evaporation.

Scanning transmission X-ray microscopy. The time-dependent magnetic configuration of the samples was investigated with time-resolved scanning transmission X-ray microscopy at the PolLux (X07DA) endstation of the Swiss Light Source³⁷. In this technique, monochromatic X-rays, tuned to the Co L_3 absorption edge (photon energy of about 781 eV), are focused using an Au Fresnel zone plate with an outermost zone width of 25 nm onto a spot on the sample, and the transmitted photons are recorded using an avalanche photodiode as detector. To form an image, the sample is scanned using a piezoelectric stage, and the transmitted X-ray intensity is recorded for each pixel in the image. The typical images we employed for the investigation of the spin-wave propagation in our samples were acquired with a point resolution between 40 nm and 75 nm.

Magnetic contrast in the images is achieved through the X-ray magnetic circular dichroism (XMCD) effect, by illuminating the sample with circularly polarized X-rays. As the XMCD effect probes the component of the magnetization parallel to the wave vector of the circularly polarized X-rays, the samples were mounted to achieve a 30° orientation of the surface with respect to the X-ray beam, allowing us to probe the in-plane component of the magnetization.

The time-resolved images were acquired in a pump-probe scheme, using an RF magnetic field of amplitude around 1 mT, generated by injecting an RF current in a microstrip antenna as pumping signal and the X-ray flashes generated by the synchrotron light source as probing signal. The pumping signal was synchronized to the 500 MHz master clock of the synchrotron light source (i.e., to the X-ray flashes generated by the light source) through a field programmable gate array (FPGA) setup. Due to the specific requirements of the FPGA-based pump-probe setup installed at the PolLux endstation, RF frequencies of $f_{\text{exc}} = 500 \times M/N$ [MHz], being N a prime number and M a positive integer, were accessible. For the measurements presented in this work, N was typically selected to be equal to 23, giving a phase resolution of about 15° in the time-resolved images. Depending on the RF frequency, the temporal resolution of the time-resolved images is given by $2/M$ [ns], with its lower limit given by the width of the X-ray pulses generated by the light source (i.e., about 70 ps FWHM).

Micromagnetic simulations. Micromagnetic simulations of the magnetization dynamics were carried out by solving the Landau–Lifshitz–Gilbert equation of motion, using the open-source, GPU-accelerated software MuMax3. The total simulated volume had dimensions of $20,480 \times 2560 \times 20 \text{ nm}^3$ and of $10,240 \times 5120 \times 20 \text{ nm}^3$ for the straight and the curved wall, respectively, and was discretized into cells having dimensions of $5 \times 5 \times 20 \text{ nm}^3$. Periodic boundary conditions in the x -direction were used to reproduce an infinite domain wall. The following parameters for the CoFeB were used: saturation magnetization $M_s = 800 \text{ kA m}^{-1}$, in-plane uniaxial anisotropy constant $K_u = 10^3 \text{ J m}^{-3}$ with the easy direction parallel to the x -axis (see Fig. 4 in the main text) and exchange constant $A_{\text{ex}} = 2 \times 10^{-11} \text{ J m}^{-1}$. The Gilbert damping parameter was set to $\alpha = 0.02$. The exchange bias field was modeled as an external magnetic field of 2.5 mT, applied along the x -axis in opposite direction inside and outside the patterned area. In order to simulate the transition between two

domains with opposite exchange bias, a 250 nm wide transition region with zero exchange bias field was placed in correspondence of the domain wall.

To simulate the spatial profile of the spin-wave modes, for both the straight and the curved wall the magnetization dynamics was excited applying a time-varying sinusoidal magnetic field to one line of cells at the center of the rectangular region and parallel to the y -axis. The field amplitude was 30 mT. In the simulation of the dispersion relation of the straight wall, in order to excite spin-waves, we used a sinc-shaped field pulse $b(t) = b_0 \frac{\sin(2\pi f_0(t-t_0))}{2\pi f_0(t-t_0)}$ directed along the x -axis, with amplitude $b_0 = 30 \text{ mT}$ and frequency $f_0 = 5 \text{ GHz}$. The dispersion relation was calculated by performing a Fourier-transform of the x -component of the magnetization both in space and time in the whole simulated area.

Data availability

The data that support the findings of this study are available from the corresponding author upon reasonable request.

Received: 29 March 2018 Accepted: 17 August 2018

Published online: 20 September 2018

References

- Chumak, A. V., Vasyuchka, V. I., Serga, A. A. & Hillebrands, B. Magnon spintronics. *Nat. Phys.* **11**, 453–461 (2015).
- Kruglyak, V. V., Demokritov, S. O. & Grundler, D. Magnonics. *J. Phys. D: Appl. Phys.* **43**, 264001 (2010).
- Wang, Q. et al. Reconfigurable nanoscale spin-wave directional coupler. *Sci. Adv.* **4**, e1701517 (2018).
- Csaba, G., Papp, Á. & Porod, W. Perspectives of using spin waves for computing and signal processing. *Phys. Lett. A* **381**, 1471–1476 (2017).
- Lenk, B., Ulrichs, H., Garbs, F. & Münzenberg, M. The building blocks of magnonics. *Phys. Rep.* **507**, 107–136 (2011).
- Urazhdin, S. et al. Nanomagnonic devices based on the spin-transfer torque. *Nat. Nanotechnol.* **9**, 509–513 (2014).
- Wintz, S. et al. Magnetic vortex cores as tunable spin-wave emitters. *Nat. Nanotechnol.* **11**, 948–953 (2016).
- Kruglyak, V. V. & Hicken, R. J. Magnonics: experiment to prove the concept. *J. Magn. Magn. Mater.* **306**, 191–194 (2006).
- Lee, K.-S. & Kim, S.-K. Conceptual design of spin wave logic gates based on a Mach–Zehnder-type spin wave interferometer for universal logic functions. *J. Appl. Phys.* **104**, 53909 (2008).
- Neusser, S. & Grundler, D. Magnonics: spin waves on the nanoscale. *Adv. Mater.* **21**, 2927–2932 (2009).
- Lee, K.-S., Han, D.-S. & Kim, S.-K. Physical origin and generic control of magnonic band gaps of dipole-exchange spin waves in width-modulated nanostrip waveguides. *Phys. Rev. Lett.* **102**, 127202 (2009).
- Kim, S.-K., Lee, K.-S. & Han, D.-S. A gigahertz-range spin-wave filter composed of width-modulated nanostrip magnonic-crystal waveguides. *Appl. Phys. Lett.* **95**, 82507 (2009).
- Khitun, A., Bao, M. & Wang, K. L. Magnonic logic circuits. *J. Phys. D: Appl. Phys.* **43**, 264005 (2010).
- Chumak, A. V., Serga, A. A. & Hillebrands, B. Magnon transistor for all-magnon data processing. *Nat. Commun.* **5**, 4700 (2014).
- Xing, X., Pong, P. W. T., Åkerman, J. & Zhou, Y. Paving spin-wave fibers in magnonic nanocircuits using spin-orbit torque. *Phys. Rev. Appl.* **7**, 54016 (2017).
- Khitun, A. & Wang, K. L. Nano scale computational architectures with spin wave bus. *Superlattices Microstruct.* **38**, 184–200 (2005).
- Kostylev, M. P., Serga, A. A., Schneider, T., Leven, B. & Hillebrands, B. Spin-wave logical gates. *Appl. Phys. Lett.* **87**, 153501 (2005).
- Kozhevnikov, A., Gertz, F., Dudko, G., Filimonov, Y. & Khitun, A. Pattern recognition with magnonic holographic memory device. *Appl. Phys. Lett.* **106**, 142409 (2015).
- Jeong, D.-E., Han, D.-S. & Kim, S.-K. Refractive index and Snell’s law for dipole-exchange spin waves in restricted geometry. *Spin* **1**, 27–31 (2011).
- Vogt, K. et al. Spin waves turning a corner. *Appl. Phys. Lett.* **101**, 42410 (2012).
- Davies, C. S. et al. Towards graded-index magnonics: steering spin waves in magnonic networks. *Phys. Rev. B: Condens. Matter Mater. Phys.* **92**, 20408 (2015).
- Sadovnikov, A. V. et al. Spin wave propagation in a uniformly biased curved magnonic waveguide. *Phys. Rev. B* **96**, 60401 (2017).
- Stigloher, J. et al. Snell’s law for spin waves. *Phys. Rev. Lett.* **117**, 37204 (2016).
- Vogt, K. et al. Realization of a spin-wave multiplexer. *Nat. Commun.* **5**, 3727 (2014).
- Haldar, A., Kumar, D. & Adeyeye, A. O. A reconfigurable waveguide for energy-efficient transmission and local manipulation of information in a nanomagnonic device. *Nat. Nanotechnol.* **11**, 437–443 (2016).

26. Garcia-Sanchez, F. et al. Narrow magnonic waveguides based on domain walls. *Phys. Rev. Lett.* **114**, 247206 (2015).
27. Lan, J., Yu, W., Wu, R. & Xiao, J. Spin-Wave Diode. *Phys. Rev. X* **5**, 41049 (2015).
28. Xing, X. & Zhou, Y. Fiber optics for spin waves. *NPG Asia Mater.* **8**, e246–e248 (2016).
29. Wagner, K. et al. Magnetic domain walls as reconfigurable spin-wave nanochannels. *Nat. Nanotechnol.* **11**, 432–436 (2016).
30. Albisetti, E. et al. Nanopatterning reconfigurable magnetic landscapes via thermally assisted scanning probe lithography. *Nat. Nanotechnol.* **11**, 545–551 (2016).
31. Albisetti, E. et al. Nanopatterning spin-textures: a route to reconfigurable magnonics. *AIP Adv.* **7**, 055601 (2017).
32. Aliev, F. G. et al. Localized domain-wall excitations in patterned magnetic dots probed by broadband ferromagnetic resonance. *Phys. Rev. B Condens. Matter Mater. Phys.* **84**, 144406 (2011).
33. Winter, J. M. Bloch wall excitation. Application to nuclear resonance in a bloch wall. *Phys. Rev.* **124**, 452–459 (1961).
34. Sharma, P. P., Albisetti, E., Monticelli, M., Bertacco, R. & Petti, D. Exchange bias tuning for magnetoresistive sensors by inclusion of non-magnetic impurities. *Sensors* **16**, 1030 (2016).
35. Albisetti, E. & Petti, D. Domain wall engineering through exchange bias. *J. Magn. Magn. Mater.* **400**, 230–235 (2016).
36. Sluka, V. et al. Stacked topological spin textures as emitters for multidimensional spin wavemodes. In *IEEE International Magnetics Conference (INTERMAG), Beijing*, 11–15 (IEEE, New York, 2015).
37. Raabe, J. et al. PolLux: a new facility for soft x-ray spectromicroscopy at the swiss light source. *Rev. Sci. Instrum.* **79**, 113704 (2008).

Acknowledgements

The research leading to these results has received funding from the European Union's Horizon 2020 research and innovation programme under grant agreements no. 705326, project SWING, and no. 730872, project CALIPSOplus. We acknowledge the support from the Office of Basic Energy Sciences of the US Department of Energy (grant no. DE-SC0016204), the US Army Research Laboratory and the US Army Research Office (grant no. W911NF-16-1-0113), and the US National Science Foundation. This work was partially performed at Polifab, the micro- and nano-technology center of the Politecnico di Milano. Part of this work was performed at the PolLux (X07DA) endstation of the Swiss Light Source, Paul Scherrer Institut, Villigen, Switzerland. The PolLux endstation

was financed by the German Minister für Bildung und Forschung (BMBF) through contracts 05KS4WE1/6 and 05KS7WE1.

Authors contributions

E.A. and D.P. conceived and designed the experiments. E.R. and R.B. supervised the research work. E.A. performed the tam-SPL patterning and data analysis. D.P. and G.S. fabricated the samples. E.A., D.P., G.S., S.F., S.W. and J.R. performed the STXM measurements. E.A., R.S. and S.T. performed the simulations. E.A., D.P., S.T. and R.B. wrote the manuscript. A.C. and X.Z. helped to setup the tam-SPL nanofabrication tool. All the authors contributed to discussions regarding the research.

Additional information

Supplementary information accompanies this paper at <https://doi.org/10.1038/s42005-018-0056-x>.

Competing interests: The authors declare no competing interests.

Reprints and permission information is available online at <http://npg.nature.com/reprintsandpermissions/>

Publisher's note: Springer Nature remains neutral with regard to jurisdictional claims in published maps and institutional affiliations.



Open Access This article is licensed under a Creative Commons Attribution 4.0 International License, which permits use, sharing, adaptation, distribution and reproduction in any medium or format, as long as you give appropriate credit to the original author(s) and the source, provide a link to the Creative Commons license, and indicate if changes were made. The images or other third party material in this article are included in the article's Creative Commons license, unless indicated otherwise in a credit line to the material. If material is not included in the article's Creative Commons license and your intended use is not permitted by statutory regulation or exceeds the permitted use, you will need to obtain permission directly from the copyright holder. To view a copy of this license, visit <http://creativecommons.org/licenses/by/4.0/>.

© The Author(s) 2018